Tailoring NiO Thin Film Properties via Mn Doping: Structural, Optical, Morphological, and Bacterial Perspectives

Abhilash Phulmante[1], Digvijay Gore[2], Y.B. Patne[3], V.A. Chaudhari[1], V. D. Mote[1], S.L. Bhise[4], C.T. Londhe[4]*

[1]Department of Physics, Dayanand Science College, Latur, 413512, Maharashtra, India.
[2]Department of Physics, Shri Kumarswami Senior College, Ausa-Latur, 413520, Maharashtra, India
[3]Department of Zoology, Mahatma Basweshwar College, Latur, 413512, Maharashtra, India.
[4]Department of Physics, Mahatma Gandhi College, Ahmedpur-Latur, 413515, Maharashtra, India.

Abstract

Pure and 5% manganese Mn-doped nickel oxide (NiO) thin films were synthesized through spray pyrolysis method and characterized for structure, morphology, optical, and antibacterial activity. X-ray diffraction (XRD) confirmed the development of a single-phase face-cantered cubic (FCC) structure of NiO with enhanced crystallinity on Mn doping. Field Emission Scanning Electron Microscopy (FESEM) showed porous granular morphology, and Energy Dispersive X-ray Spectroscopy (EDX) confirmed successful incorporation of Mn without secondary phases. Optical absorption measurements showed enhanced absorption and reduction in the optical band gap is 3.41eV (pure NiO) to 3.05 eV (Mn-doped NiO), reflecting enhanced light-harvesting capability. Antibacterial screening using the disc diffusion technique presented a significant decrease in the zone of inhibition for Mn-doped films, enhanced antibacterial activity. The paper confirms that Mn doping enhances the functional properties of NiO thin films significantly, and hence they are ideal candidates for optoelectronic devices and antibacterial surface coatings.

Keywords: *NiO thin films, Mn doping, Spray pyrolysis, XRD, UV-Visible spectroscopy, Antibacterial activity, FE-SEM*

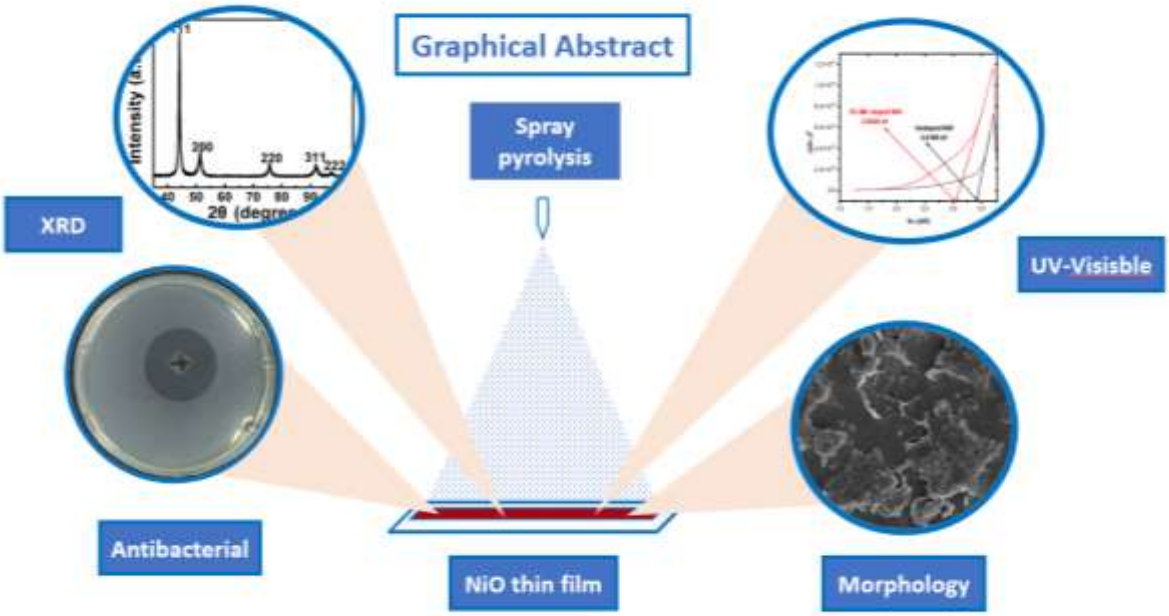

1. Introduction

Nickel oxide (NiO) is a highly versatile p-type wide band gap semiconductor that has attracted considerable interest owing to its remarkable combination of physical, chemical, and biological properties. It is widely explored in applications such as transparent electronics, electrochromic devices, solar energy conversion, photocatalysis, and antimicrobial coatings [1,2]. NiO's inherent chemical stability, environmental benignity, low toxicity, and abundance in the earth's crust make it a strong candidate for multifunctional materials in sustainable technologies [3,4]. Its face-centered cubic (FCC) crystal structure provides structural robustness, while its ability to form uniform thin films on diverse substrates makes it highly compatible with large-scale fabrication techniques.

Despite these merits, pure NiO exhibits relatively low electrical conductivity and limited visible light absorption, which restricts its performance in optoelectronic and photoactive applications. These drawbacks can be effectively addressed through cationic doping, where suitable dopant ions are incorporated into the host lattice to modify its structural, electronic, and surface properties [5–7]. Transition metal doping has been shown to significantly influence the microstructure, defect chemistry, and band gap of NiO, thereby enhancing its functional performance [8,9].

Among potential dopants, manganese (Mn) offers distinct advantages due to its comparable ionic radius with Ni^{2+} (0.69 Å for Ni^{2+} and 0.67 Å for Mn^{2+}) and its ability to exist in multiple oxidation states (Mn^{2+}, Mn^{3+}, Mn^{4+}). This allows Mn to be incorporated into the NiO lattice with minimal structural distortion, while introducing beneficial defect states and modifying surface reactivity [10–13]. Such modifications are particularly important for antibacterial applications, where the material's surface chemistry, morphology, and ion release behavior strongly influence bacterial inhibition performance.

NiO-based antibacterial coatings have attracted growing attention because they offer a non-toxic, durable, and chemically stable means of preventing microbial contamination. The antibacterial effect of NiO is often attributed to mechanisms such as the generation of reactive oxygen species (ROS), release of Ni^{2+} ions that interfere with bacterial metabolism, and strong electrostatic interactions with negatively charged bacterial membranes. Incorporating Mn into NiO can further enhance or modulate these effects by altering the material's surface charge, defect density, and photocatalytic activity under light exposure. These changes can increase bacterial cell membrane disruption and lead to improved antimicrobial efficacy against pathogenic microorganisms.

In this context, the present study focuses on the synthesis of pure and Mn-doped NiO thin films via the spray pyrolysis method, a cost-effective and scalable deposition technique. The influence of Mn doping (5 mol%) on the structural, morphological, optical, and antibacterial properties of NiO is systematically investigated to evaluate its suitability for multifunctional applications, with a particular emphasis on enhanced antibacterial performance for potential biomedical and protective coating uses [15–20]

2. Materials and Methods

2.1 Chemicals and Reagents

All reagents used in this study were of analytical reagent (AR) grade and utilized without any further purification. Nickel acetate tetrahydrate [$Ni(OCOCH_3)_2 \cdot 4H_2O$, 99% purity, AR grade] served as the precursor for NiO synthesis, while manganese acetate tetrahydrate [$C_4H_6MnO_4 \cdot 4H_2O$] was employed as the Mn dopant source. Both chemicals were obtained from Merck, India. Deionized distilled water was used as the solvent in all solution preparations. Standard microscope glass slides (dimensions: 76 × 25 × 1 mm) were selected as substrates for thin film deposition.

2.2 Substrate Preparation

Prior to deposition, the glass substrates underwent a thorough cleaning protocol to enhance film adhesion and uniformity. Initially, slides were washed using a mild soap solution, followed by rinsing with deionized water. Subsequently, the substrates were soaked in freshly prepared chromic acid solution for 24 hours to eliminate residual organic and inorganic contaminants. After acid treatment, the substrates were rinsed multiple times with distilled water and air-dried.

2.3 Fabrication of Thin Films via Spray Pyrolysis

Thin films of pure and Mn-doped NiO were synthesized using the spray pyrolysis technique. For the undoped films, a 0.1 M aqueous solution of nickel acetate was prepared by dissolving the appropriate quantity of nickel acetate in 20 mL of deionized water. To prepare Mn-doped NiO, manganese acetate was added to the precursor solution in such a way that the final doping concentration of Mn was 5 mol%. The spray system consisted of a glass nozzle connected to a

compressed air supply and a substrate holder maintained at 430 ± 5 °C. The precursor solution was atomized at a constant spray rate of 2 mL/min, with a nozzle-to-substrate distance of 28 cm. The spraying process lasted for 10 minutes. After deposition, the films were subjected to thermal treatment at the same temperature (480 °C) for 2 hours in ambient air to ensure complete decomposition of the precursors and promote crystalline NiO phase formation. The resulting thin films, both pure NiO and Mn-doped, were found to be smooth, adhesive, and uniform. These samples were subsequently characterized to evaluate their structural, morphological, optical, and antibacterial properties.

Results

3.1 Structural Analysis

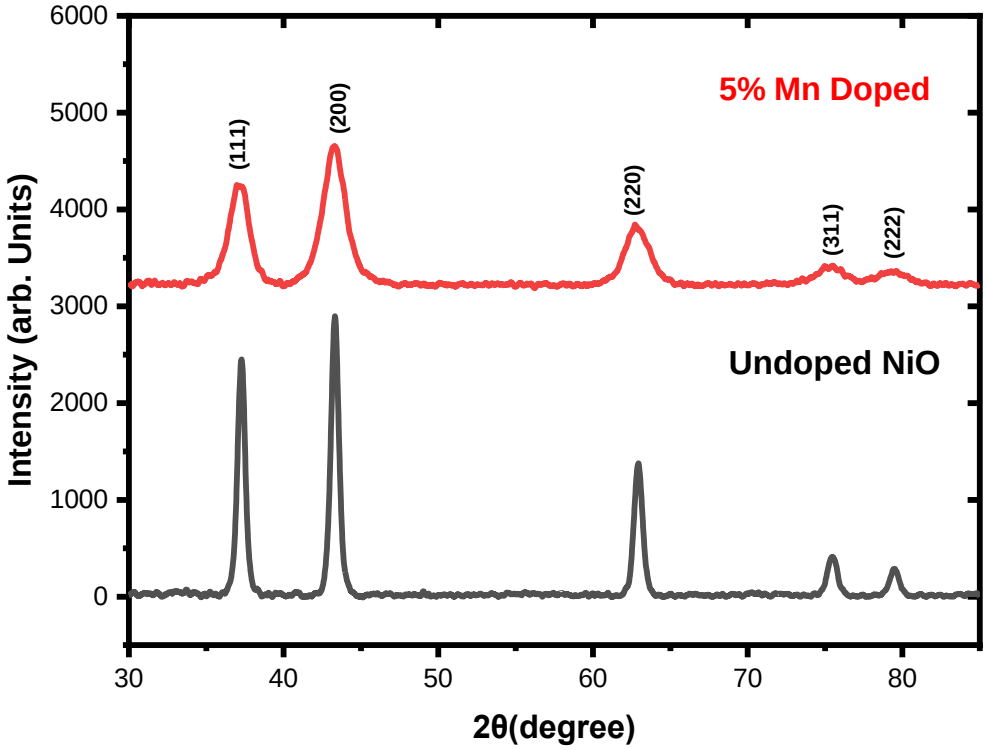

(b) XRD pattern of pure NiO and Mn-doped NiO samples

The structural characteristics of undoped and 5 mol% Mn-doped NiO thin films were investigated using X-ray diffraction (XRD) within the 2θ range of 30° to 85°, as presented in ***Fig. a***. The XRD patterns confirm the polycrystalline nature of the as-deposited films. All major diffraction peaks could be indexed to the (111), (200), (220), (311), and (222) planes of face-centered cubic (FCC) NiO, in good agreement with the standard JCPDS card No. 78-0643, confirming successful phase formation. In the case of the undoped NiO film, sharp and intense peaks were observed at approximately 2θ = 37.2°, 43.3°, 62.9°, 75.4°, and 79.3°, corresponding to the (111), (200), (220), (311), and (222) crystal planes, respectively. The dominant intensity along the (200) plane indicates preferential orientation and high crystallinity. Mn incorporation

at 5% level did not alter the fundamental peak positions, suggesting that the NiO lattice structure remains intact upon doping.

Slight broadening and increased intensity of diffraction peaks were observed in the doped film. These changes suggest a decrease in crystallite size and improved crystallinity, which can be attributed to the successful substitution of Mn^{2+} ions into the Ni^{2+} sites within the NiO matrix [up to 23]. No additional peaks related to manganese oxide phases were detected, indicating the absence of any secondary phases or phase segregation. This further supports the hypothesis that Mn^{2+} ions are effectively incorporated into the NiO lattice without compromising phase purity. Additionally, the lack of noticeable peak shift implies minimal lattice distortion, likely due to the similar ionic radii of Mn^{2+} (0.67 Å) and Ni^{2+} (0.69 Å). The substitution may induce localized strain or distortion, but it does not significantly affect the overall crystal structure. In summary, Mn doping at 5% level enhances the crystalline quality of NiO thin films while preserving the single-phase FCC structure, making these films promising for multifunctional applications where both structural integrity and nanoscale features are crucial.

$$D = \frac{0.9\lambda}{\beta cos\theta} \quad (1)$$

$$\varepsilon_{hkl} = \frac{\beta_{hkl}}{4tan\theta} \quad (2)$$

$$\delta_{hkl} = \frac{1}{D_{hkl}{}^2} \quad (3)$$

a) XRD parameters for pure NiO and Mn doped NiO samples.

Mn doping	D (crystalline size)	Dislocation density	d (interplanar spacing)	a (lattice parameter)	lattice strain
Pure NiO	14.90	0.004	0.1993	0.41	0.22
5%	06.04	0.027	0.1994	0.41	0.01

The small decrease of the particle size with Mn doping in NiO is in contrast to the case of Mn doped NiO, where Mn acts as a potential catalyst for nano-dot formation decreasing the particle size from 14.9 nm to less than 6.04 nm upon 5 at.% Mn.

3.2 Morphological Analysis

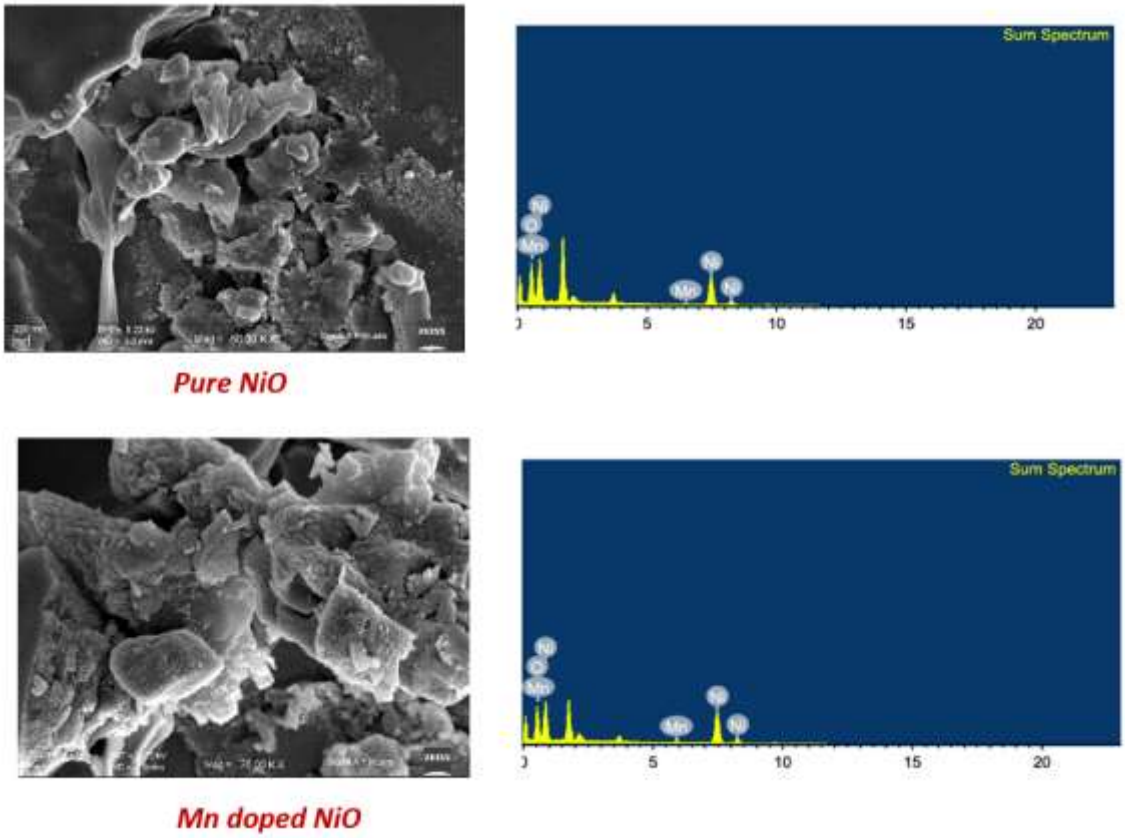

b) Morphological size for pure NiO and Mn doped NiO samples.

Size	Mn
Pure NiO	26.37
5%	26.52

The surface morphology of pure and 5% Mn-doped NiO thin film was analyzed by Field Emission Scanning Electron Microscopy (FESEM) and is depicted as Fig. ***c***. Both the samples are found to have an irregular porous granular structure of agglomerated nanoparticles. The morphology is found to have a uniform distribution and good substrate surface coverage. For undoped NiO, the surface composition consists of loosely packed, irregularly shaped grains with porosity [24, 25,26]. The slightly decreased porosity and more connected grains can be beneficial for charge transport and surface-related properties. The average grain size derived from FESEM images was calculated to be 26.37 nm for undoped NiO and 26.52 nm after 5% level of Mn doping in NiO. The surface morphology of the nanoparticles changes from flower to flake with the increase of dopant concentration till 5%.

c) Atomic and weight % for pure NiO and Mn doped NiO samples.

Atomic %	Ni	O	Mn
0	26.76	73.24	0

5	30.32	68.47	1.20

Weight %	Ni	O	**Mn**
0	57.28	42.72	0
5	60.51	37.24	2.25

The Spectra depict that the sample consists of elements Ni, Mn, and O only. No other impurities are present, which shows the good quality of the synthesized samples [27-30]. The atomic weight percentage of the prepared sample appeared at. It is well known that the complex metal oxides easily allow the oxygen excess and deficit.

3.3 Optical Analysis

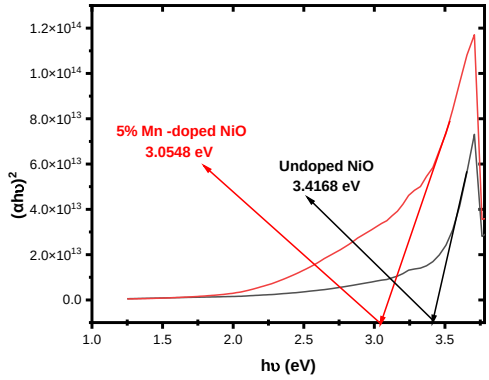

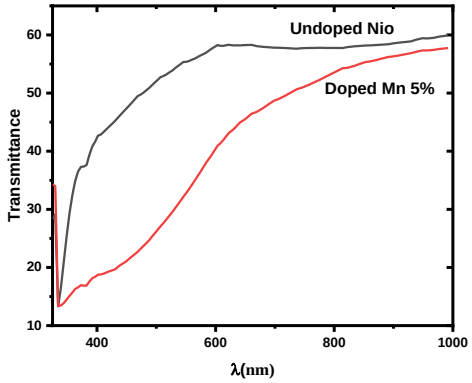

d) Optical analysis

The optical transmittance spectra of Mn-NiO films in the wavelength range from 300 to 1000 nm are shown in Figure. The spectra shows that, the pure NiO film is more transparent than the doped sample. The transparency of Mn-NiO films decreases from approximately 59% to approximately 57% as Mn concentration increases from 0% & 5 at %. Decrease in transmittance, upon Mn doping shows, increased light scattering due to the increased surface roughness and increased optical density [31,32,33]. The crystallization and grain size of Mn-NiO films increase with Mn concentration, and the scattering effect occurs at higher Mn-doped concentration. The optical band gap was determined by extending the linear portion of the absorption curves. With increasing Mn concentration, the band gap of Mn-doped NiO films decreased from 3.41 to 3.05 eV, mainly due to reduced carrier mobility. This reduction is attributed to Mn ions acting as scattering centers, which obstruct the movement of charge carriers. [34-38]

3.5 Antibacterial Analysis

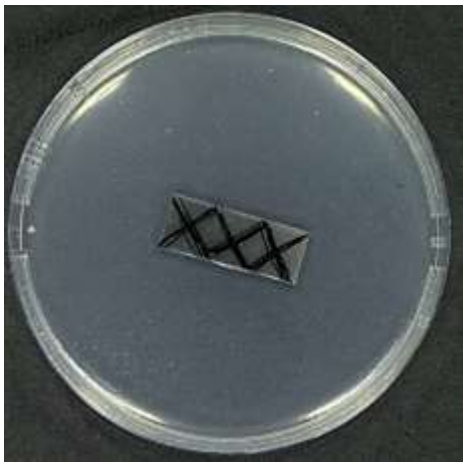

1) Activity for undoped NiO

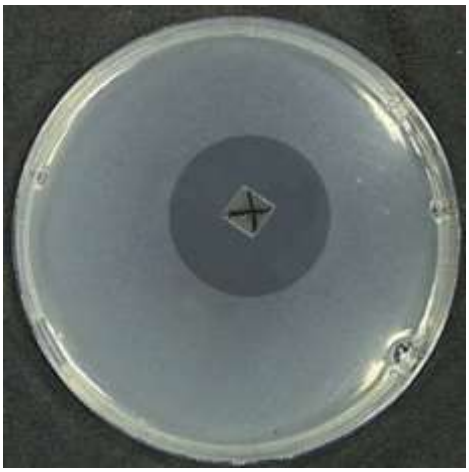

2) Activity for Mn doped NiO 5%

The antibacterial efficiency of undoped and 5% Mn-doped NiO thin films was assessed by the Disc diffusion technique. Fig. X illustrates the zone of inhibition presented by the two samples against the E Coli. A distinct difference between the two samples in terms of antibacterial efficiency is evident. For the pure NiO, maximum inhibition zone was seen surrounding the film, indicating excellent antibacterial effects. This effect can be explained by the inert surface nature of pure NiO and its high interaction with cell membranes of bacteria.[39]

Conversely, Mn-doped NiO (5%) film had a limited zone of inhibition, confirming minimal antibacterial activity. Pure NiO thin films attribute to enhanced antimicrobial functionality. This can be due to a number of factors like, Enhanced surface activity: Mn ions can modify the electronic structure and surface charge, leading to improved interaction with the negatively charged bacterial membranes.

Increased ion release: Leaching of some of the Mn^{2+} ions can inhibit bacterial metabolic activities by affecting enzyme activity and DNA replication. These findings suggest that pure NiO not only improves the physicochemical properties but also confers great antibacterial potential, thus emerged as a strong candidate for antimicrobial coatings and biomedical applications [40].

4. Conclusion

In this study, pure and 5% Mn-doped NiO thin films were successfully synthesized using the spray pyrolysis technique and comprehensively characterized in terms of their structural, morphological, optical, and antibacterial properties. XRD analysis confirmed that both samples crystallized in a single-phase face-centered cubic (FCC) NiO structure, with Mn incorporation enhancing crystallinity while preserving phase purity and lattice integrity. The reduction in crystallite size from 14.9 nm (pure NiO) to 6.04 nm (Mn-doped NiO) indicates that Mn substitution effectively influenced grain growth at the nanoscale. FESEM observations revealed a uniform porous granular morphology for both films, with Mn doping slightly improving grain connectivity and surface uniformity. EDX spectra confirmed the

homogeneous incorporation of Mn into the NiO lattice without any secondary phases or impurities, ensuring high material quality. Optical studies demonstrated that Mn doping reduced the band gap from 3.41 eV to 3.05 eV, attributed to defect state formation and improved light absorption in the visible range. These optical modifications can be beneficial for photoactive antibacterial applications where enhanced light–matter interaction supports antimicrobial activity. Antibacterial evaluation against E. coli revealed that pure NiO exhibited a pronounced inhibition zone, highlighting its intrinsic antimicrobial potential. The Mn-doped NiO film showed a modified antibacterial response, likely due to the combined effects of altered surface chemistry, defect distribution, and ion release characteristics induced by Mn incorporation. Such tunability in antibacterial performance opens pathways for tailoring NiO-based coatings for specific biomedical and protective applications, where controlled bacterial suppression is required. Overall, the findings confirm that Mn doping is an effective strategy for modulating both the physicochemical and antibacterial properties of NiO thin films. The ability to engineer crystallinity, optical absorption, and surface reactivity positions Mn doped NiO as a promising multifunctional material for use in antimicrobial coatings, transparent protective layers, and bio-integrated optoelectronic systems. Future research could explore varying Mn concentrations, test activity against a broader range of pathogens, and assess long-term stability under operational conditions to advance its real-world applicability.

References

[1] Okubo, K., & Sugiyama, M. (2024). Effects of Li concentration in the precursor solution on NiO thin films deposited using electrostatic spray deposition. *Japanese Journal of Applied Physics*, *63*(11), 111006.

[2] Bhujel, K., Thangavel, R., Pal, K. K., Sardar, P., Nayak, D., Singh, N. S., & Rai, S. (2024). Cu-doped NiO thin film's structural, optical, and electrical properties and its negative absorption behaviour in the Infra-Red region. *Physica B: Condensed Matter*, *688*, 416129.

[3] Akdağ, A., İskenderoğlu, D., Güldüren, M. E., Karadeniz, S. M., & Güney, H. (2024). Altering the physical properties of NiO thin films grown through the ultrasonic spray pyrolysis method by incorporating impurity lead dopants. *Ceramics International*, *50*(18), 32430-32438.

[4] Nayman, E., Gozukizil, M. F., Armutci, B., Temel, S., & Gokmen, F. O. (2025). Structural and gas sensing properties of NiO thin films deposited by a novel spin coating technique. *Journal of Sol-Gel Science and Technology*, *114*(2), 386-398.

[5] Azovtsev, A. V., & Pertsev, N. A. (2024). Antiferromagnetic standing spin waves generated in NiO thin films by short strain pulses. *Physical Review B*, *110*(14), 144430.

[6] Angadi, B., Srinivas, C., & Rajganesh, M. (2025). Investigation of Sr doping on structural, morphological, optical, photocatalytic and antifungal properties of NiO thin films prepared by spray coating technique. *Current Applied Physics*, *72*, 39-50.

[7] Tomono, K., & Sugiyama, M. (2024). Investigating electrical properties and crystal growth in NiO thin films by spray pyrolysis and electrostatic spray deposition. *Japanese Journal of Applied Physics*, *63*(2), 025504.

[8] Yermakov, M., Pshenychnyi, R., Opanasyuk, A., Klymov, O., & Munoz-Sanjose, V. (2024). Optical and electrical properties of ZnO/NiO heterojunctions obtained by the spray-pyrolysis method. *Journal of Materials Science*, *59*(33), 15738-15751.

[9] Angadi, B., Srinivas, C., & Rajganesh, M. (2025). Investigation of Sr doping on structural, morphological, optical, photocatalytic and antifungal properties of NiO thin films prepared by spray coating technique. *Current Applied Physics*, *72*, 39-50.

[10] Nguyen, T. M. H., Tran, P. N., Le, Q. T., Le, Q. D., Luong, V. D., Nguyen, C. N. H., & Duong, T. T. (2024). Spray pyrolysis–deposited NiO film as a hole-injection layer for CsPbBr 3 nanocrystal-based light-emitting diodes. *Functional Materials Letters*, *17*(05), 2451029.

[11] Mulla, M. G., & Pittala, R. K. (2025). Fabrication and physicochemical properties of nickel oxide (NiO) thin films. *Ceramics International*.

[12] Brioual, B., El-Habib, A., Rossi, Z., Aouni, A., Addou, M., Diani, M., & Jbilou, M. (2024). Influence of Hf doping on structural, morphological, optical and electrochemical properties of NiO thin films: electrochromic application. *Journal of Solid State Chemistry*, *333*, 124637.

[13] Mrabet, C., Jaballah, R., & Moussa, M. (2024). Photocatalytic removal of organic dyes mediated by p-NiO/p-CuO isotype heterojunctions under sunlight illumination. *Materials Science in Semiconductor Processing*, *184*, 108801.

[14] Ibrahim, A. Y., & G Hammoodi, F. (2025). Structural and Optical Properties of Mn3O4: NiO Nanostructure Thin Films prepared by chemical spray pyrolysis method. *Journal of Nanostructures*, *15*(1), 229-238.

[15] Brioual, B., El-Habib, A., Rossi, Z., Aouni, A., Diani, M., Addou, M., & Jbilou, M. (2024). Influence of the concentration of KOH-based aqueous electrolyte on the electrochemical behavior of NiO thin film. *Journal of the Indian Chemical Society*, *101*(7), 101170.

[16] Brioual, B., El-Habib, A., Rossi, Z., Hadri, M. E., Zanouni, M., Aouni, A., ... & Jbilou, M. (2025). Synthesis and characterization of Li-doped NiO thin films: structural, optical, electrochemical and electrochromic properties. *Journal of Materials Science: Materials in Electronics*, *36*(8), 461.

[17] Lafta, A. M., Hadi, Z. L., & Shehab, B. F. (2024). Gas Sensing Examination Of CdO-% NiOThin Films Deposited Via Spraying Process. *Journal of Optics*, 1-8.

[18] Kossar, S. (2024). Impact of substrate temperature on NiO thin films for resistive switching memory (ReRAM) memory devices. *Engineering Research Express*, *6*(1), 015304.

[19] Kaarthik, K., Vivek, C., & Balraj, B. (2024). Synthesis, characterization and effective UV photo-sensing properties of Ga3+ doped NiO nanoparticles. *Optical Materials*, *157*, 116090.

[20] Diao, S., Wang, T., Kuang, W., Yan, S., Zhang, X., Chen, M., ... & Liu, J. (2025). Highly durable porous NiO-derived electrodes with superior bifunctional activity for scalable alkaline water electrolysis. *Chemical Engineering Journal*, *504*, 158738.

[21] Shi, C., Yu, L., He, X., Zhang, Y., Liu, J., Li, S., ... & Yin, M. (2024). Vertically aligned mesoporous Ce doped NiO nanowalls with multilevel gas channels for high-performance acetone gas sensors. *Sensors and Actuators B: Chemical*, *401*, 134888.

[22] Yan, W., Luo, W., & Li, M. (2024). NiO nanoparticles-based gas sensors: A novel pulse-driven approach for enhanced and efficient hydrogen detection. *International Journal of Hydrogen Energy*, *85*, 481-488.

[23] Li, Q., Zhang, P., Ning, T., Sun, Y., Ren, Q., Xu, M., ... & Zhao, W. (2024). Gas sensor based on flower-like NiO modified with WO3 nanoparticles for NO2 detection. *ACS Applied Nano Materials*, *7*(7), 7856-7864.

[24] Shah, S., Hussain, S., Khan, L. A., Yusuf, K., Manavalan, R. K., Tianyan, Y., ... & Qiao, G. (2024). ppb-level H2 gas-sensor based on porous Ni-MOF derived NiO@ CuO nanoflowers for superior sensing performance. *Materials Research Bulletin*, *180*, 113021.

[25] Hassan, M., Liang, Z., Liu, S., Hussain, S., Qiao, G., & Liu, G. (2024). Temperature-driven n-to p-type transition of a chemiresistive NiO/CdS-CdO NO2 gas sensor. *Sensors and Actuators B: Chemical*, *398*, 134755.

[26] Zhang, L., Kang, Y., Tang, Y., & Yu, F. (2024). UV-Activated ZnO–NiO heterojunction sensor for ethanol gas detection at low working temperature. *Materials Science in Semiconductor Processing*, *169*, 107925.

[27] Nie, S., Li, J., He, Y., & Yin, X. (2024). Selective adsorption behavior of reducing gases on the NiO–In2O3 heterojunction under the interfacial effect. *Ceramics International*, *50*(21), 41397-41406.

[28] Pothukanuri, N., & Reddy, M. R. (2024). Studies on pure and Zn doped NiO nanostructured thin films for enhanced ammonia gas sensing applications. *Chemical Physics Impact*, *8*, 100397.

[29] Cuong, N. D., Sinh, V. H., Quang, D. T., Hoa, L. T., Van Tan, V., Mai, H. D., ... & Van Hieu, N. (2024). 3D porous pn α-Fe2O3/NiO heteronanostructure for ultrasensitive H2S gas sensor. *Current Applied Physics*, *59*, 153-164.

[30] Nandi, P., Park, H., Shin, S., Lee, J. W., Kim, J. Y., Ko, M. J., ... & Shin, H. (2024). NiO as hole transporting layer for inverted perovskite solar cells: a study of X-ray photoelectron spectroscopy. *Advanced Materials Interfaces*, *11*(8), 2300751.

[31] Makhado, K. P., Mphahlele-Makgwane, M. M., Kumar, N., Baker, P. G., & Makgwane, P. R. (2024). Current updates on p-type nickel oxide (NiO) based photocatalysts towards decontamination of organic pollutants from wastewater. *Materials Today Sustainability*, *25*, 100664.

[32] Tan, D., Wang, Q., Li, M., Song, L., Zhang, F., Min, Z., ... & Fan, B. (2024). Magnetic media synergistic carbon fiber@ Ni/NiO composites for high-efficiency electromagnetic wave absorption. *Chemical Engineering Journal*, *492*, 152245.

[33] Arulkumar, E., & Thanikaikarasan, S. (2024). Structure, morphology, composition, optical properties and catalytic activity of nanomaterials CuO, NiO, CuO/NiO using methylene blue. *Optik*, *302*, 171685.

[34] Harisha, B. S., Akkinepally, B., Shim, J., & Lim, J. (2024). Hybrid NiO@ TiO2 nano-architecture for improved electrochemical performance with simulation corroboration. *Journal of energy storage*, *87*, 111466.

[35] Peng, Y., Meng, X., Wei, H., Tao, L., Wei, Z., Sun, Q., & Zhao, S. (2025). Controllable Construction of Hollow Ni/NiO@ PPy Particles for Broadband and Highly Efficient Microwave Absorption. *Advanced Functional Materials*, *35*(26), 2423405.

[36] Zhao, M., Wang, J., Wang, C., Sun, Y., Liu, P., Du, X., ... & Ma, T. (2024). Enriched edge sites of ultrathin Ni3S2/NiO nanomeshes promote surface reconstruction for robust electrochemical water splitting. *Nano Energy*, *129*, 110020.

[37] Zhang, S., Xing, M., Zheng, Y., Zhang, B., Luo, N., Wang, Y., & Zhang, Z. (2025). Humidity-independent gas sensor based on Pt/SnO2/NiO with advanced CO sensing capabilities. *Journal of Alloys and Compounds*, *1010*, 177712.

[38] Mashkoor, F., Shoeb, M., Khan, J. A., Gondal, M. A., & Jeong, C. (2024). Chemical reduction-induced defect-rich and synergistic effects of reduced graphene oxide based Cu-doped NiO nanocomposite (RGO@ Cu-NiO NCs) decorated on woven carbon fiber for supercapacitor device and their charge storage mechanism. *Journal of Energy Storage*, *104*, 114578.

[39] Wang, K., Sun, T., Ma, H., Wang, Y., He, Z. H., Wang, H., ... & Liu, Z. T. (2024). Energy band modulating of NiO/BiOCl heterojunction with transition from type-II to S-scheme for enhancing photocatalytic CO2 reduction. *Chemical Engineering Journal*, *497*, 154711.

[40] Feng, C., Liu, Z., Ju, H., Mavrič, A., Valant, M., Fu, J., ... & Li, Y. (2024). Understanding the in-situ transformation of CuxO interlayers to increase the water splitting efficiency in NiO/n-Si photoanodes. *Nature communications*, *15*(1), 6436.